A Spatio-Temporal *in-situ* Investigation of the Payne Effect in Silica-Filled Rubbers in Large Amplitude Oscillatory Extension.

Mariapaola Staropoli*[a], Dominik Gerstner[b], Benoit Duez[b], Michael Sztucki[d], Guido Vehres[c], Aurel Radulescu[c], Jean-Sébastien Thomann[a], Stephan Westermann[a], Wim Pyckhout-Hintzen[c]

[a] Luxembourg Institute of Science and Technology – 41, Rue du Brill, L-4422 – Belvaux (Luxembourg)

[b] Goodyear S.A. – Avenue G.T. Smith, L-7750 – Colmar-Berg (Luxembourg)

[c] Forschungszentrum Jülich – Jülich Centre for Neutron Science 1 - Leo-Brandt-Straße – D-52428 Jülich (Germany)

[d] ESRF Grenoble – 71, Avenue des Martyrs, F-38000 – Grenoble (France)

ABSTRACT

The present work deals with the structural and dynamic characteristics of a silica filler network within an industrial elastomeric composite with time-resolved USAXS, collected for the first time *in-situ* under periodic uniaxial deformation. The *in-situ* configuration allows a unique correlation between the x-ray patterns highlighting the structure of the filler and the dynamic-mechanical stress-strain response that characterizes the full composite. A scattering model is applied to quantitatively identify the filler network evolution as a function of dynamic strain. To address the Payne effect and the underlying structural modifications correlated to intra- and inter-filler-aggregate effects, all rubbers were pre-conditioned to suppress stress-softening related to the Mullins effect. Sector-averaged scattering intensities along the parallel strain direction reveal a jamming/de-jamming transition between clusters. The dynamic stress response of the full composite shows onsets of non-linear behavior and a contribution of higher harmonics of the fundamental excitation frequency.

1. INTRODUCTION

Filler-reinforced rubbers find applications in many industrial sectors and especially in the automotive and tire industry. Their enhanced elastic modulus resulting from the addition of rigid and clustering nanofillers to the rubbery matrix is often described by a hydrodynamic reinforcement mechanism [1-3]. The addition of non-deformable particles into a rubbery system, besides giving rise to the reinforcement on the molecular level, causes a considerable constraint on the surrounding polymer dynamics [4-6]. These multiple polymer-filler and filler-filler interactions are as well responsible for a complex mechanical response when the filled elastomer is exposed to a deformation, depending on the amplitude of the applied strain [4, 7, 8]. The strain-induced breakage of the percolating filler network is indeed known to have a strong impact on the mechanical properties, causing reversible and irreversible changes of the internal structure of the composite and a reduction of the elastic response of the material. The commonly occurring phenomenon at intermediate-to-large deformations is the so-called Mullins effect observed especially for filled rubbers under multi-cyclic deformation [9, 10]. There, a mostly irreversible stress softening process mainly appearing during the first strain cycles of quasi-static deformation results in a hysteretic stress-strain behavior. This

phenomenon is commonly described by the Dynamic Flocculation Model (DFM) that relies on the assumption of a diffusion-controlled aggregation of the particles [11]. Original and reversibly re-formed clusters exhibit thereby different strengths upon unloading. Many phenomenological, micromechanical and constitutive modeling approaches and pertinent to these strain levels have been proposed basing on various combinations of springs and dashpots [12-15]. Low strains, on the other hand, invoke another mechanical effect, termed as the Payne effect. Under oscillatory deformation with increasing dynamic amplitude, filled rubbers exhibit a strongly non-linear dependence of the dynamic moduli on the amplitude and, specifically, evidence a drop of the elastic modulus at high deformation. The Payne effect is known to be related to the reversible filler-filler bond breakage at small strains that strongly impacts the mechanical performances of filled elastomers and is the main cause of rolling resistance in tires [16-19]. The Kraus model was handled for a long time as a description of the Payne effect by the continuous breakage and reformation of filler bond [20] and was favored over another approach by Maier-Göritz [21]. The empirical models are, however, limited to the linear strain domain only and cannot be applied to the case of high amplitudes. Lion and co-workers have presented an interesting and inspiring approach based on continuum mechanics for the dynamic stress behavior of pre-deformed rubbers [17, 22]. However, the investigation of the Payne effect as in relationship to the filler-matrix interaction and thus to the structural changes occurring within the filler network upon strain requires the synergy of studies on microscopic and macroscopic scale. The application of x-ray and neutron scattering methods with *in-situ* deformation is known to provide significant details on the filler network arrangement within the rubbery environment [23]. The study here presented deals with the evolution of the hierarchical highly dispersible silica (HDS) filler network in Styrene-Butadiene rubbers (SBR) under an oscillatory deformation in the non-linear regime. To our best knowledge, this study represents the first dynamic-mechanical and time-resolved experiment performed *in-situ* in the x-ray beam yielding direct information on filler network response to the dynamic strain. In specific, this work was conducted through ultra-small angle x-ray scattering (USAXS), assisted with small angle neutron scattering (SANS) and with parallel *in-situ* dynamic-mechanical stress responses on the macroscopic level in large-amplitude-oscillatory-extension (LAOE) mode. While the development of the filler network under the application of large tensile strains typical for the Mullins mechanism has been largely addressed [24-30], we only focus here on the effect of an oscillatory deformation on the filler structure that corresponds to the small-amplitude Payne effect. With the aim of addressing the Payne effect solely and observing the underlying structural modifications correlated to intra- and inter-filler-aggregate effects, all rubbers were pre-conditioned to suppress residual irreversible stress softening related to the large strain Mullins effect. The choice of large-amplitude-oscillatory-extension (LAOE) applied so far in a limited number of studies [31, 32] over the more commonly applied large-amplitude oscillatory shear tests (LAOS) [33, 34] is connected to the importance of a large extension amplitude for the understanding of the mechanical behavior of rubber in modus operandi [32] and the development of materials with high mechanical performance and reduced mechanical loss [16, 35]. The present work proposes, in addition, a quantitative description of the scattering-mechanical results on the bases of a previously published scattering model [30] and a recently developed procedure [36] allowing the subtraction of the ZnO parasitic contribution from the scattering function. In literature few works presented a *quantitative* identification of the hierarchical structures of the fillers during a ramping-up deformation. Many reported investigations focus, however, on the development of anisotropic 2D scattering images [24-27, 29, 37, 38]. In this case, we propose a different approach which aims to the quantitative correlation of the structural evolution with the sinusoidal strain, rather than the modelling of the full scattering curves.

As we will show, the simultaneous application of time-resolved stroboscopical scattering and mechanical measurements gives unique access to a time-dependent evolution of the clusters shape under large-amplitude oscillatory extension (LAOE). This spatio-temporal approach is an elegant tool for structure-property relationships. Especially, the synergy of scattering and mechanics has the unique advantage of identifying the effect of the deformation on the fillers only. We introduce a

simplified intensity ratio to identify the microscopic response of the filler to avoid evaluation of statistical noisy data on top of the needed catalyst corrections.

Within the present article, the effect of rubber functionalization and the amount of rubber-filler silane coupling agent on the structural evolution of silica clusters and their mechanical response are reported. A quite recent study on the microscopic level of the Payne effect dealing with different matrix-filler interactions has been reported in the literature [19]. In the cited work, the structural and mechanical properties of filled paraffin oil and filled SBR were compared. It was evidenced that the Payne effect is principally related to the filler network reorganization, while the polymer-matrix interaction has a secondary effect. A thermal dependence of the Payne effect was however observed in the case of the SBR. Within our work, we aim at the understanding of the matrix functionalization effect on the filler dispersion and on their response to the applied dynamic deformation. The combination of a scattering model function with the oscillatory deformation profile identifies a deviation from the affine behavior, which is found to be strongly correlated to the matrix functionalization level. This deviation from affine response is furthermore connected to a so-called jamming phenomenon, associated with structural arrest of the dynamics by the percolation of rigid fillers [39, 40]. The mechanical response in LAOE shows first signatures of an onset of non-linear behavior and the occurrence of higher odd and even harmonics from a Fourier analysis. The specific modelling of the filler-related scattering data allows a clear distinction of the fillers and polymer contribution to the total mechanical response.

2. EXPERIMENTAL

2.1 Nanocomposites preparation. The styrene-butadiene rubber (SBR) used in this work has a medium styrene (21%) / high vinyl (62%) micro-structure and a typical glass transition temperature of -25 °C. Solution-polymerized SBR is pre-mixed with an aromatic distillate oil Treated Distillate Aromatic Extract (TDAE). The "fn polymer" bears functionalization targeted to improve silica-polymer interaction, the “non-fn polymer” does not have functional groups to specifically interact with silica. The random copolymers were mixed with highly dispersible silica (HDS) with specific surface of $165.8\ m^2/g$ (N2 BET). Samples with silica loading of 90 phr were prepared in a standard way using an internal mixer of the Banbury type followed by a two-roll milling process. Rubber and fillers were mixed in a non-productive stage using bis-3-triethoxysilylpropyldisulfide (TESPD) as coupling agent. The amount of silane coupling agent varies among the samples studied. In this stage N-(1,3)-dimethylbutyl-N-phenyl-p-phenylenediamine (6-PPD) was used as antioxidant while N-cyclohexyl-2-benzothiazolesulfeneamide (CBS) and diphenylguanidine (DPG), respectively, were added as first and secondary accelerators. During the productive stage, the curing package was introduced. In this stage, the temperature was kept <120°C and the sulfur and stearic acid curing package as well as ZnO curing activators was introduced. For all the compounds $10x10\ cm^2$ sheet samples (thickness ~ 0.7 mm) were obtained by compression-molding vulcanization. Three samples with different rubber functionalities and variable silane amount were used. Samples studied in this work are classified in Table 1.

	FN POLYMER-HDS	FN POLYMER-HDS-10phf	NON-FN POLYMER-HDS
SSBR (fn polymer)	100	100	
SSBR (non-fn polymer)			100
HDS	90	90	90

Silane (TESPD)	7.2	9	7.2
TDAE oil	25	25	25
Stearic Acid	3	3	3
6-PPD	2.5	2.5	2.5
ZnO	2.5	2.5	2.5
Sulfur	1.4	1.4	1.4
CBS	2.3	2.3	2.3
DPG	3.2	3.2	3.2

Table 1: Sample classification. The amount of each component is reported in phr.

2.2 Dynamic Mechanical Analysis (DMA). Dynamic mechanical data in Large Amplitude Oscillatory Extension (LAOE) mode were obtained *in-situ* during the USAXS experiment using a home-built tensile device, developed at Forschungszentrum Jülich (FZJ), installed at the sample position of the USAXS beamline (ID02). Several oscillatory dynamic deformation amplitudes between 1 and 20% peak-to-peak were applied to the samples. However, since an appreciable variation in the scattering pattern can be identified starting from above 5% sinusoidal amplitude, only results for the 8% and 20% amplitude will be taken into account in the data evaluation. Forced oscillatory motion with a frequency of 0.25 Hz allows *in-situ* data collection from a load cell with 50N capacity in both tension and compression. For the present experiments, an initial uniaxial loading cycle was applied to sample strips of 5 x 1 x 0.06 cm^3 length-to-width-to-thickness between the clamps up to 100% of the initial length at a cross-head speed of 0.2 mm/s. The deformation was reversed from 100% to 0 with an identical strain rate in order to remove the Mullins effects, followed by a ramping-up to a fixed pre-strain of 30%. Every 0.025 s the motor positions and tensile forces were recorded, yielding 160 force data per cycle, over a time period of 80s i.e. 20 cycles. The average force corresponding to the pre-strain at t=0 was subtracted to obtain pure dynamic stresses. No measurable stress relaxation over 80s could be noticed. Dynamic moduli and phase angle could be extracted as in the linear case.

The in-situ DMA instrument is designed primarily for neutron small angle scattering experiments at the MLZ facility in Garching and is included as a special sample-environment-equipment within the control software of the KWS2 diffractometer. It is a modified version of an elongational set-up used in former neutron scattering studies of stretched melts in quenched state and ideally suited for larger deformations [41-43]. A new temperature box in analogous design to classical commercial rheometers like ARES (Rheometrics Ltd, TA Instruments) is constructed around the sample position and can be easily removed for measurements at room temperature or modified for other non-scattering techniques. Neutron-transparent Quartz glass (ULTRASIL) windows in entrance and beam exit can be replaced by other materials depending on the scattering probe. For X-rays, X-ray-transparent materials like Kapton are favored. Metallic sheets with pre-drilled holes taking advantage of the high collimation and the intrinsic strongly reduced size of the X-ray beam (<0.1mm in X-ray vs approximatively 10cm diameter in neutron case) are possible as well. Underneath the thermobox a load cell is included in the static cylinder while the upper cylinder is freely moveable.
Three deformation modes are currently enabled: a linear strain profile (constant speed of the upper clamp, ideal for rubbers), an exponential strain profile (constant strain rate with exponentially increasing speed of deformation, ideal for un-crosslinked melts and extensional rheometry) and a sinusoidal variable strain profile around a variable preset or pre-stretch. Strain profiles can be pre-programmed in a sequence file and applied continuously or cyclically to the rubbers.
The control of the machine is done by means of a Labview-based procedure and combines the motion and measurements of the parameters as travelled distance, temperature, offsets, forces.

2.3 Ultra Small Angle X-ray Scattering (USAXS). Time resolved Ultra small-angle X-ray scattering (USAXS) measurements were performed at ID02 of the ESRF Grenoble [44] at 31 m detector distance, and λ = 1 Å with q= (4π/λ) sin θ/2, where θ is the scattering angle. To synchronize USAXS data acquisition with the DMA recording, the beam line hardware sent a TTL pulse that started the strain device movement and acquisition. The relation between time scales defined for the beam line and DMA data was subject to an uncertainty, as a certain delay between the sending of the TTL pulse and actual start of the DMA acquisition can be expected. By comparing the time series, the maximum delay was estimated to ~100 ms. The q-range covered varies from 10^{-4} to 0.1 $Å^{-1}$. To synchronize maximally with the rheometer, the detector was kept blind in the continuous beam always for 0.24s and scattering data recorded thereafter during 0.01s and repeated. For each period 16 time-channels are thus obtained, in total 320 over 80 s, corresponding to 20 periods for each deformation amplitude. The data presented in the next paragraph are related to the 5^{th} period only for each sinusoidal deformation. The choice of the 5^{th} period is connected to the minimization of artefacts like the settling of the waveform from rest and minimal relaxation of the stress with evolving time. For absolute scaling of the intensities to cm^{-1} units, the scattering of water was used. Transmission, background, as well as thickness corrections were performed through the SAXS Utilities software. Incompressibility was assumed for the varying thicknesses and transmissions. Sectors with opening angles of ±5° were applied to 2D scattering images along the vertical and horizontal directions of the scattering intensities. These sectorial averages were obtained for both the deformed and non-deformed states since considerable anisometric states were identified in the non-stretched samples. The quantitative evolution of the cluster size has been obtained in terms of ratio of the intensities measured at each channel and the initial one, corresponding to zero dynamic deformation. The ratio of the different channels here analyzed, only relates to the scattering intensity measured along the vertical axes, coinciding with the strain axes. This procedure allows the identification of defined values for the cluster size variation with the deformation direction.

2.4 Small Angle Neutron Scattering (SANS). Selected SANS experiments were conducted at the KWS-2 diffractometer of MLZ, (Garching, Germany) [45] using a detector distance of respectively 20 m at a wavelength of 10 Å. The scattering vector range spanned between about $10^{-3} < q < 0.01$ $Å^{-1}$. 2D-detector data were obtained in 142 x 142 channels of 8 x 8 mm2 size. The wavelength distribution $\Delta\lambda/\lambda$ was 10%. For the absolute scaling to absolute units [cm^{-1}] the incoherent scattering level of a secondary standard Plexiglass was used. The data were corrected pixelwise for empty beam scattering, detector sensitivity, and background noise using B_4C as beam blocker and subsequently radially averaged. In the case of anisotropic scattering patterns, sectors with total opening angles of 10° along the main axes of the anisotropic patterns were applied to the scattering patterns. Static strains were chosen as to yield structural comparison in the dynamic USAXS data to be able to perform the ZnO correction.

3. MODEL DESCRIPTION

Substantial efforts have been made in the past to correlate relationships between mechanical responses and the microscopic structures of viscoelastic polymers and filled rubbers as we investigate here. Oscillatory stress responses intrinsically contain more information than the quasistatic stress-strain analysis. In the latter, a quasi-static equilibrium with vanishing dynamic contributions is approximated by a slow but continuous stretching of the samples. While quasistatic stress-strain testing is the standard to test filled rubbers in e.g. Rubber Process Analyzer (RPA) instruments, large amplitude oscillatory stress responses are much less commonly measured. In shear mode the rubbers

Eq. 1

are placed between two plates and the resulting displacement is usually symmetric around the quiescent state. The observed stress response is therefore symmetric. In the case of a sinusoidal shear strain signal $\gamma(t)$, the resulting stress response $\tau(\gamma(t), t)$ is in the same way sinusoidal but shifted in time over a phase angle δ. The periodic amplitude is defined as:

$$\gamma(t) = \gamma_o \sin(\omega t)$$

where $\gamma(t)$ and γ_o correspond to the dynamic strain and the modulated amplitude. The symmetric dynamic stress response is thus defined as:

$$\tau(+\gamma, t) = -\tau(-\gamma, t)$$

$$\tau(t) = \tau_0 \sin(\omega t + \delta) = \tau_0 \left(\mathrm{G}'\sin(\omega t) + G"cos(\omega t)\right) \quad \textbf{Eq. 2}$$

The periodical stress function can be decomposed in a Fourier series consisting of sine and cosine functions. A Fourier transformation of the time-dependent stress (or modulus) would yield therefore both in-phase and out-of-phase components and the phase angle δ , defined as $\delta = \tan^{-1} G''/G'$. For small amplitude strains around the rest state, the stress-to-strain is a linear relationship and one single phase angle can be identified. Large shear amplitudes give rise to a more complex response, consisting of higher harmonics. For rubber, large amplitudes are predominantly reserved to tensile experiments (LAOE). A non-linear stress signal as function of the strain is expected. In addition, the application of a pre-strain that exceeds the dynamic extensional amplitude of the oscillatory strain is required for keeping the rubber in the stretched state [46]. A direct consequence of the tensile deformation is the deviation from the symmetric shape of the stress amplitude due to the different stress value in the maximum and minimum of the cycle, comparable to the stress values in the stress-strain curves.

At relatively low dynamic strain amplitudes, after the subtraction of the static pre-stress from the total signal, close-to-ellipsoidal dynamic stress vs strain hysteresis loops are obtained. However, non-linear responses arising from higher dynamic strain amplitudes result into distorted shapes at the extremes. In shear (LAOS) such large amplitude oscillatory experiments in the non-linear regime showed that only odd harmonics due to symmetry are needed for a full description of the stress response [47]. In the non-symmetric case, as for the extensional deformation, both odd and even harmonics are expected to appear [34]. For LAOE, the stress σ as function of time is expressed as:

$$\sigma(t) = \sigma(\varepsilon_p) + \varepsilon_0 \sum_{m=1}^{N} \sin(m\omega t + \delta) = \sigma(\varepsilon_p) + \varepsilon_0 \sum_{m=1}^{N} a_m \sin(m\omega t) + b_m \cos(m\omega t) \quad \textbf{Eq. 3}$$

Here, a and b are the weighting factor parameters i.e. the in-phase and out-of-phase moduli, while ε_p and ε_0 represent respectively the static pre-strain and the dynamic amplitude. The harmonics are contained in m. The parameters m and the π/2-shifted cosine functions determine the appearance of a distorted stress response. The number of harmonics as well as their contributions depending on the pre-factors can be obtained through a discrete Fourier transform while the amplitude of each contributing frequency is proportional to the complex modulus [48]. A description of non-linear stress-strain responses of nanocomposites in LAOE and LAOS has been reported in the literature [31, 32]. In the present work, we will limit our investigation to a simplified quantitative analysis of the oscillating stress, while numerical structural parameters will be obtained in the modelling of the scattering results.

Differently from DMA which yields the full dynamic response of the composite particle-filled rubber, the USAXS or SANS signal arises from the spatial fluctuation of scattering length density between the particle and matrix that lead to a scattering contrast. The scattering function reflects an ensemble-averaged system consisting of time- and deformation-dependent parameters. Therefore, the chosen

approach of combining high-intensity SAXS obtained typically from a synchrotron source or SANS with DMA is a selective tool for correlating the structural changes occurring in the composite with mechanical properties simultaneously in a large amplitude sinusoidal tensile strain experiment around a certain pre-strain. As Payne effects are assigned to the filler aggregates structure, this work aims at the development of structure-property relations for Mullins-devoid silica filled SBR rubbers with different functionalization. In the quasi-static analysis proposed in our former work, the scattering model based on the work of Teixeira was used to describe interacting and associating silica particles [30, 49, 50]. The evaluation of the USAXS results in relation to the mechanical behavior required a correction for the parasitic scattering of ZnO catalyst beforehand. All experimental USAXS data at low *q* in the present work are corrected using a Guinier function of the ZnO particle, the radius of which is ~ 450 Å, as determined in a previous work through the combination of USAXS and SANS tests [36]. The USAXS *q*-range smaller than 10^{-3} Å^{-1}, distinct from the SANS region, is eventually affected as well by void and agglomerate scattering. The length scales here involved are those of voids and inhomogeneities and the experimental *q*-dependence is typically between q^{-4} and q^{-2}. Both void scattering and clusters that are linked into fractal agglomerate networks contribute to this low-*q* region. The missing overlap of scattering vectors in SANS and USAXS experiments impedes a total correction of the results for the ZnO contribution. In addition, the subtraction of these contributions would lead to unpredictable variation of the *q*-region of interest, where the clusters have the major contribution. The subtraction of the ZnO contribution here applied allows, however, the best-possible correction of the data in the *q* range $3 \cdot 10^{-3} - 8 \cdot 10^{-3}$ Å^{-1}, which is dominated by the cluster contribution and it is the *q*-region of interest for this investigation. For the correction procedure as well as the hierarchically based scattering model, we refer to previous publications. Here we investigate the affinity in the small strain limit.

The oscillatory deformation of a sample is a time-dependent function. The deformation ratio is defined as:

$$\lambda(t) = \frac{L(t)}{L(0)} = 1 + \varepsilon(t) \qquad \textbf{Eq. 4}$$

Where $L(t)$ and $L(0)$ are the actual and initial length of the sample between the clamps of the stretching rheometer. The total time-dependent strain $\varepsilon(t)$ consists of two contributions: the static pre-strain ε_p and the dynamic sinusoidal strain with amplitude ε_0 and frequency *f*.

$$\varepsilon(t) = \varepsilon_p + \varepsilon_0 \cdot \sin(\omega t) = \varepsilon_p + \varepsilon_0 \cdot \sin(2\pi f \cdot t) \qquad \textbf{Eq. 5}$$

Thus, also the total deformation is a time-dependent relation. If $\varepsilon_d(t)$ represents the dynamic part of the strain, Eq. 4 and 5 can be combined and re-written together to obtain:

$$\lambda(t) = \left(1 + \varepsilon_p + \varepsilon_d(t)\right) = \left(1 + \varepsilon_p\right) + \varepsilon_0 \sin(\omega t) = \lambda_p + \varepsilon_0 \sin \omega t \qquad \textbf{Eq. 6}$$

So that the deformation ratio is situated un-symmetrically between the ranges
$\lambda_p - \varepsilon_0 \leq \lambda \leq \lambda_p + \varepsilon_0$ **Eq. 7**

Now the scattering function is introduced. The scattering expression consists of a product of the cluster form factor and particle form factor, as defined within the model based on the Teixeira function. The same approach for deformed clusters in the USAXS regime is here used. The pre-factor of the Guinier function of the cluster contains the volume of the cluster as ~ ξ^D where D is the mass-fractal dimension and ξ the average size of the cluster.

$$\forall\, q\xi \leq 1\colon\ S(q) \sim \Gamma(D+1)\left(\frac{\xi}{R}\right)^D \exp\left(-\frac{D(D+1)(q\xi)^2}{6}\right) \qquad \textbf{Eq. 8}$$

Here, Γ is the gamma function and R the radius of the particles composing the cluster. If the sample is deformed affinely with λ , then for small *q* (i.e. large distances) in USAXS a close-to-affine behavior on the level of the clusters may be expected. Deviations from affinity in the incompressible rubber may then be due to a so-called microscopic deformation λ_{exp} where the displacement of the clusters is smaller than the effective displacement of the sample.

$$\xi \rightarrow \xi \cdot \lambda_{exp} \qquad \textbf{Eq. 9}$$

where λ_{exp} can be lower than the incompressibility-linked affine λ.

The modification of this analysis for dynamically obtained intensities can be done easily by inserting the time-dependent parameters. The scattering of the 16 time- channels that make up a full period – see experimental section for details – will be compared to that of reference channel 0 (or 16) which corresponds to zero amplitude of dynamic strain. The ratio of both, called R_{exp} further down yields the dynamic scattering response only. Furthermore, this ratio of intensities is built *q* value-by-*q* value in the *q* range ranging from $3{\cdot}10^{-3}$ to $7{\cdot}10^{-3}$ $Å^{-1}$in which the Guinier function of the cluster scattering applies. To reduce the statistical error of the ratio, all ratios were averaged and a final uncertainty of about 3% is achieved. This procedure is a practical approach and allows the number of single analyses to be reduced and different samples to be compared fast in a suitable way. We will show later that the scattering data are in phase with the macroscopic dynamic strain. The experimental and theorical ratio according to the affine assumption are then expressed relative to the pre-strain data at the beginning of each cycle, respectively as:

$$R_{exp} = < \frac{I(t)}{I(t=0)} > \qquad \textbf{Eq. 10}$$

$$R_{aff} = \frac{\xi_{iso}^{D}(1+\left(\frac{\varepsilon_0}{\lambda_p}\right)\sin(\omega t))^{D}}{\xi_{iso}^{D}} \qquad \textbf{Eq. 11}$$

The ratio, R_{exp} (USAXS) is obtained by dividing $I(\lambda(t))$and $I\left(\lambda_p\right)$ corresponding, respectively, to the intensity measured at each step/time channel of the sinusoidal deformation and the intensity measured at zero dynamic amplitude. The dependence on the initial cluster size for the theoretical affine ratio R_{aff} function, estimated for an affine displacement of the clusters with the deformation, (ξ_{iso}) in Eq. 11 cancels therefore out and the ratio is only a function of ε_0, λ_p, the radial frequency ω and the mass fractal dimension D. The exponential term is assumed to cancel out and would only lead to 2nd order corrections. Only D is thus a parameter of the system. From our former static study, the D exponent showed to be invariant to strain in the small deformation limit. This affine – or under-affine deformation should also correlate to the static experiment.

In the following section the USAXS data will be analyzed in terms of the ratios previously introduced and compared with the measured stress-strain curves.

4. RESULTS AND DISCUSSION

4.1 USAXS and SANS results: USAXS results with *in-situ* dynamic-mechanical tests are reported here for samples with different rubber functionality and silane amount. The combination of the structural and mechanical tests allows the determination of the structural evolution of clusters with applied oscillatory deformation. To conduct tensile tests in oscillatory mode, a pre-strain of 30% was applied to the samples. In a separate Small Angle Neutron Scattering (SANS) test, needed to extract the ZnO correction function, it was observed that at this initial static deformation the samples under

investigation exhibit a closest-as-possible isotropic state. While the raw 2D scattering images collected through USAXS are strongly affected by the presence of ZnO, the contribution of the curing activator to the SANS intensity is negligible. For this reason, the analysis of the x-ray data is done entirely on ZnO-corrected 1D intensities. The SANS raw 2D images reported in Figure 1 are only shown for two of the samples analyzed in this work to emphasize the isotropic state at zero-dynamic deformation and its approximate anisotropy at the extremes of the sinusoidal strain. The scattering vector shown covers the q-range $-0.02 < q < +0.02$ Å^{-1}.

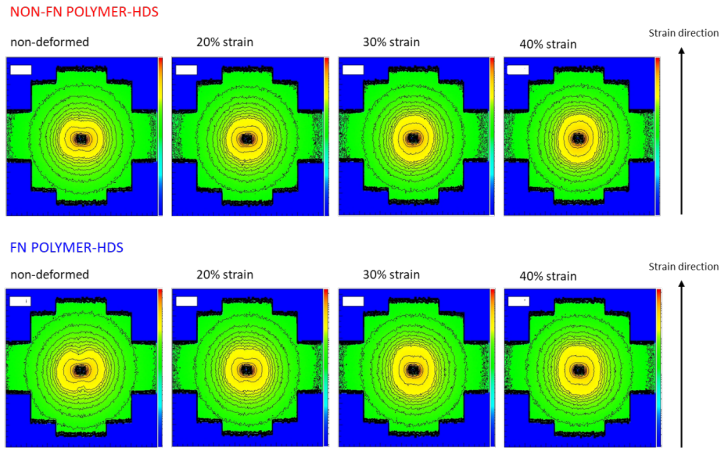

Figure 1. Representative SANS patterns from a static point of view, characterizing the extrema of the sinusoidal dynamic strain of 20% for samples NON-FN POLYMER-HDS (top) and FN POLYMER-HDS (bottom). The pattern at pre-stretch 30% can be largely considered as isotropic.

In the following we focus on the two largest dynamic amplitudes to investigate how non-linearity shows up in the structural parameters:

20% double-dynamic amplitude:

In Figure 2, 1-dimensional sector-averaged scattering intensities along the direction parallel to the oscillatory strain are shown as a function of time for NON-FN POLYMER-HDS, FN POLYMER-HDS and FN POLYMER-HDS-10phf (see Table 1 for details). The dynamic peak-to-peak amplitude corresponds to 20%. The 1D curves indicate the evolution of the scattering intensities along strain axis. The insert shown in each figure emphasizes the pattern change occurring in the interesting intermediate *q*-region, in which the clusters contribution is dominant. This evolution of the intensity indicates that, upon deformation, the clusters align or deform in-phase along the strain direction leading to an increase of the scattering intensity along the same axes. The maximum of the amplitude corresponds to the highest intensity. Sustaining consistency, all data in the q-range of the primary particle coincide. Differences between the samples, however, can be detected. For the samples containing functionalized SBR (fn polymer) the more pronounced intensity variation measured at different time channels, suggests that the cluster displacement is larger than in the case of non-functionalized matrix (non-fn polymer). In addition, for NON-FN POLYMER-HDS (Fig. 2a) the Guinier-region seems to extend to higher *q* than for FN POLYMER-HDS and FN POLYMER-HDS-10phf (Fig. 2b and 2c). The separation between parasitic void/ agglomerate scattering and cluster intensity is tentatively larger in the functionalized fn polymer matrix samples than for non-fn polymer. This is a direct indication that smaller clusters are formed when silica is mixed with functionalized SBR. The FN POLYMER-HDS-10phf

sample indicates a high filler dispersion with smaller clusters and increased coupling with functionalized matrix in parallel with a stronger intensity change when strain is applied.

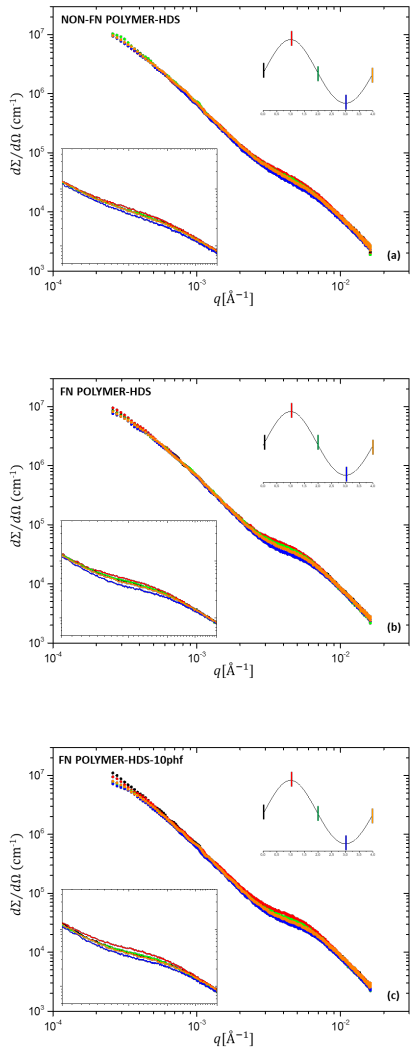

Figure 2. 1D scattering intensities for samples NON-FN POLYMER-HDS (a), FN POLYMER-HDS (b) and FN POLYMER-HDS-10phf (c) at different time channels, each corresponding to one deformation step. All curves correspond to the intensities measured along the sector parallel to the deformation.

The ratio function is reported in Figure 3, in comparison with the theoretical function estimated in the assumption of an affine spring-like response of the cluster size with the oscillatory deformation and 20% peak-to-peak amplitude. The experimental uncertainties of this macroscopic strain-derived curve are indicated by the dashed lines marking the extremes of an estimation based on the measured displacement profiles and a synchronization uncertainty (100 ms) mentioned in 2.3. This does not affect the conclusions that are drawn below.

Before the experimental ratios are discussed in more details, the following observations from Figure 3 and 4 which describe the results for the 5th cycle are required. The function R does not show an out of phase component with respect to the applied strain amplitude as seen for the angles 0, π and 2π corresponding to the times 0,2s and 4s. The answer of the fillers is basically elastic and excludes contributions from a cosine function (see Eq.3), that would result in a finite phase angle shift. Additionally, this excludes the contribution from odd harmonics. The m=2 is the only and strongest expected overtone. Depending on the relative contributions of m=2 with f=0.5Hz and P=2s the possible effects expected are related to the slopes of the R function with respect to the theoretical one. In particular, the shallower slope observed between 1 and 2s as well as between 2 and 3s effectively observed might be attributed to the m=2 contribution. Longer times are not interpreted due to other peculiarities (see below).

Commented [MS1]: New details over experimental results

The three samples studied exhibit a considerably different scattering ratio. The four quadrants of the sine wave are here discussed separately in line with the above.

Range 0-1 s: the up-phase shows different response of the clusters at 20% deformation for differently functionalized samples. For the samples containing the functionalized matrix (fn polymer) the maximum in the experimental ratio is close to the theoretical estimate (within statistical error). Sample FN POLYMER-HDS-10phf (magenta), in which the silane content is higher than in the two other cases, shows an almost affine-like value. This observation is in good agreement with a more significant interaction between the deformed rubber matrix and the silica, promoting motion of the clusters along the strain direction. The maximal ratio at 1s is in phase with the macroscopic dynamic strain, except for the sample FN POLYMER-HDS (blue) for which the maximum is shifted. The appearance of this shift could be due to structural effects induced, for instance, by the different amount of rubber occluded by the aggregates that depends on the matrix functionalization and strongly affects the response of the filler clusters to the deformation. Experimental uncertainties might contribute to the shift too and the different possible contributions will be further discussed. The ratio observed for the sample containing unfunctionalized SBR, NON-FN POLYMER-HDS (red) is clearly lower than the prediction. This is likely a consequence of the lower filler-rubber interaction and larger filler clusters.

To estimate the deviation of the scattering data from the affine prediction, the ratio:

$$SR^{+} = \frac{(R_{\exp})^{1/D} - 1}{(R_{aff})^{1/D} - 1}(1s)$$

compares the macroscopic strain and the effective or microscopic strain for the cluster deformation. The values range from $SR^{+}{\sim}0.7 - 1.1$ for FN POLYMER-HDS-10phf, $SR^{+}{\sim}0.4 - 0.6$ for NON-FN POLYMER-HDS and $SR^{+}{\sim}0.5 - 0.7$ for FN POLYMER-HDS.

Range 1-2s: For the sample FN POLYMER-HDS (blue) the experimental ratio function is observed to be out of phase in respect with the theoretical prediction. As explained above, the maximum in this case appears at 1.25 s. This shift is indicative for a retarded compliant response of the filler cluster or inter-cluster viscoelastic rearrangements. In the time range here considered, except for the peak position, the trend of the scattering ratios observed for the three different samples is in agreement with the calculated function within experimental uncertainties.

Range 2-3s: in the time range between 2s and 3s, a difference between the theoretical prediction and the experimental trend of the ratio is observed. Specifically, the absolute value of the in-phase minimum at 3s in the experimental scattering ratio is larger than the calculation for all samples here studied, indicating a clear deviation from the prediction in the compression phase also for the sample FN POLYMER-HDS-10phf (magenta).

Similar to before, the deviation of the scattering data from the prediction is estimated by:

$$SR^{-} = \frac{(R_{\exp})^{1/D} - 1}{(R_{aff})^{1/D} - 1}(3s).$$

The values range from $SR^{-}\sim 0.6-0.7$ for FN POLYMER-HDS-10phf (magenta), $SR^{-}\sim 0.6-0.7$ for NON-FN POLYMER-HDS (red) and $SR^{-}\sim 0.6-0.8$ for FN POLYMER-HDS (blue). Interestingly, these values are very similar for all the samples in this phase, indicating a possible specific arrangement of the fillers upon compression. Considerations about the structure of the fillers leading to this experimental trend will be reported in the next paragraphs.

Range 3-4s: In the reverse straining phase just before reaching the reference state again, the sample FN POLYMER-HDS (blue) shows the same time shift as in the 2nd quadrant. The minimum is reached later at 3.25s and simultaneously a lower ratio than at 3s is observed. This response seems to correspond to a higher compressibility of the clusters and to a delay in the rearrangement than in the other two samples. This discrepancy could be explained if a slower rearrangement of the particles within the clusters and larger filler cluster moving relative to each other would be is considered due to non-permanent filler-filler interactions competing with the covalent permanent rubber-filler coupling. The best dispersion with smaller clusters is achieved with increased functionalization. A different situation would be instead predicted for the sample NON-FN POLYMER-HDS (red) in which the lower rubber functionalization causes a less pronounced cluster rearrangement in comparison to the other two samples. A worse filler dispersion and larger clusters are at least expected as consequence of the reduced filler-rubber interactions induced by the non-functionalized matrix. The occluded rubber content may be larger as well.

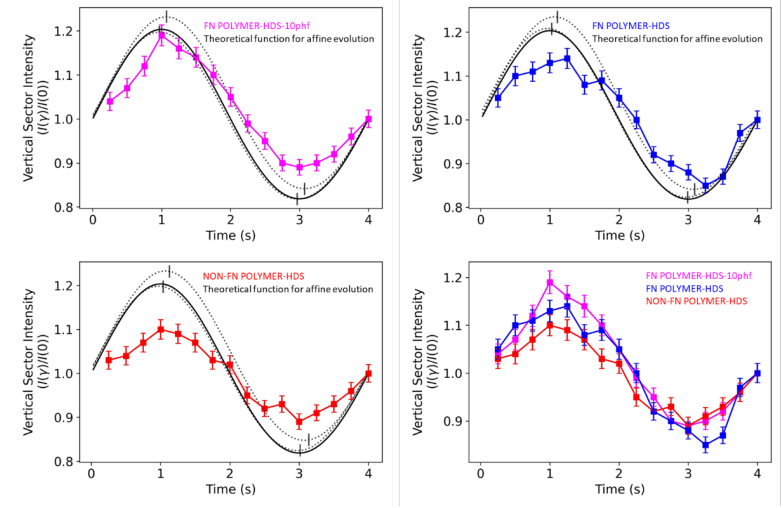

Commented [MS2]: Figure 3 and 4 were switched in the previous document.

Figure 3. Evolution of the scattering ratio with 20% amplitude oscillatory deformation along the strain direction for FN POLYMER-HDS (blue), NON-FN POLYMER-HDS (red) and FN POLYMER-HDS-10phf (magenta) as function of time in comparison with the theoretical prediction of the same ratio estimated for an affine displacement of the clusters.

While it is not surprising that the affinity assumption doesn't hold in the up-phase for the non-functionalized matrix and at least tentatively explained by a non-linear deformation of the filler cluster, the coinciding deviation in the down-phase for t > 2s requires more accurate analysis. This under-affinity can be correlated to a topological jamming phenomenon leading to an arrest of filler motion when the clusters approach each other and start to interpenetrate. It is intuitively clear that due to incompressibility a structural re-arrangement of clusters is not unlikely. In a possible scenario of packed spheres, the stretching of a densely filled percolated rubber leads to an inter-mixing with neighboring spheres. The resulting free space is ideally suited, consequently, to be occupied by adjacent or nearby particles that move along the compression direction following the incompressibility rules. The consistently lower deformation in the down-phase of the sinusoidal strain can be tentatively rationalized.

In this regard, clusters are defined as subunits of a larger filler ensemble. Therewith, both intra- and inter-cluster length scales are accessed in the used q-range. The following approximation relies on the validity of a body centered cubic (BCC) lattice model for describing the arrangement of such clusters within the agglomerate, as schematically represented in Scheme 1. From the filling degree of 90phr or corresponding volume fraction of ~ 30% the necessary geometrical parameters of the unit cell can be defined as a consequence of the "dilution" of the packing. The volume fraction of the involved two particles in the expanded BCC unit cell is defined as:

$$\phi = \frac{2 \cdot \frac{4}{3}\pi \cdot {R_p}^3}{a^3} \qquad \textbf{Eq. 12}$$

Where a is the edge length of the cube or distance between the centres-of-mass of the corner particles and R_p is the average radius of the particles. The average distance between the surfaces of the two corner particles is indicated by Δ.

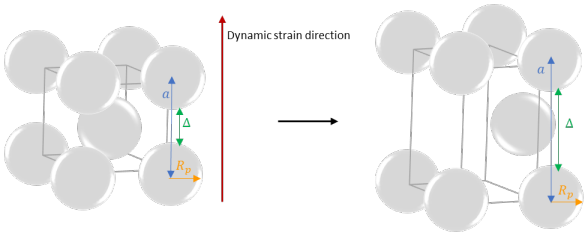

Scheme 1: Schematic view of fillers particles in a BCC cubic system and tentative representation of the displacement of fillers within one cell under the action of an asymmetric compressive force perpendicular to the strain.

From Eq. 12, the relationship between the parameters a and R_p can be obtained as:

$$\frac{{R_p}^3}{a^3} = 0.036 \Rightarrow a = 3.03 R_p \qquad \textbf{Eq. 13}$$

For the non-deformed state Δ is estimated as $\Delta = a - 2R_p \approx 1.03\ R_p$. If the unit cell is deformed affinely by the pre-strain of 30% then the distance a increases as $a = 3.03R_p \cdot 1.3 = 3.94\ R_p$, while $\Delta = 1.94\ R_p$.

At this deformation level, the interparticle surface-to-surface distance is lower than the diameter of a particle. The compressive force in the perpendicular direction to the pre-strain has as sole consequence that any pre-orientation of the fillers is destroyed. This evidence was shown in the SANS images of Figure 1, where the 2D scattering images reported exhibit a transition from anisotropic to isotropic distribution. In the up-phase of the dynamic deformation, at a deformation ratio corresponding to λ= 1.4, the total distance can be estimated as $a = 3.03R_p \cdot 1.4 = 4.24\ R_p$ which corresponds to a surface-to-surface distance of $4.24\ R_p - 2R_p = 2.24\ R_p$. In this case, the particles belonging to near unit cells or the center particle itself can occupy the free space under the effect of the compression force exerted in the direction perpendicular to the deformation, following the incompressibility law. The free space between adjacent particles along the strain direction becomes higher than $2R_p$, allowing therefore the rearrangement of the unit cell as tentatively represented in Scheme 2. The free space between the surfaces of two particles figuratively collocated along the edge of one cube reduces to $0.123\ R_p$. In the down-phase, however, the reorganization of this new configuration is undefined. The surfaces of the adjacent particles can get in contact again or the forced reduction of uniaxial strain may expel the newly-inserted particle. The simplified description here used cannot predict the rearrangement of the filler network in this phase.

The experimental values of scattering ratio at the maximum and minimum of the dynamic amplitude can be estimated as following:

$$R^+ = \left(1 + \frac{A}{1.3}\right)^D \qquad \textbf{Eq. 14}$$

$$R^- = \left(1 - \frac{A}{1.3}\right)^D \qquad \textbf{Eq. 15}$$

from Eq. 11. Here, R^+ and R^- are the extremes of the ratio function at a certain dynamic amplitude A. The parameter D is the mass fractal and 1.3 corresponds to the static deformation applied as the pre-strain.

From Figure 3, the experimental R^- is found at approximately 0.92 for the samples FN POLYMER-HDS-10phf and NON-FN POLYMER-HDS, in strong contrast to the affine prediction of $R^- = 0.82$.

Assuming a value of $D = 2.5$, as determined experimentally [30] the effective dynamic amplitude at this minimum can be estimated as $A = 0.053$ that corresponds to $\lambda = (1.3 - 0.053) = 1.25 \pm 0.02$. The strain thus is -0.053. The discrepancy between this value and the theoretical prediction based on the affine assumption, suggests an arrest of the particles dynamics that do not follow the rubber in the down phase of the deformation. The interruption of the configuration rearrangement at this strain is a signature of a jamming effect induced by the combination of static and dynamic deformation. The jamming observed in this case is related to geometrical factors rather than thermodynamic processes observed in glasses. It is worth noting that sample FN POLYMER-HDS showing a different R^- is found closer to the theoretical value which occurs at approximately 3,25 s rather than at 3 s. The higher displacement of the fillers along the strain direction in the samples containing functionalized rubber can, at the same time, lead to a slower rearrangement of the cluster conformation upon strain. The jamming-unjamming transition may have an un-explored effect which is not described by higher harmonics. The compression seems to introduce a fragile, transient penetration or interdigitation of clusters or cluster parts that, once separated, behave “normal’ again in the following up-phase. While

the sample FN POLYMER-HDS-10phf contains also the functionalized SBR rubber, the higher amount of silane that is responsible for the more affine-like behavior in comparison to FN POLYMER-HDS might as well lead to the earlier arrest of the dynamics in the reverse strain phase. This observation can be related to the higher cross-linking degree within the rubber induced by the enhanced silane content [51] that might hinder the rearrangement of the clusters after they are displaced along the strain direction.

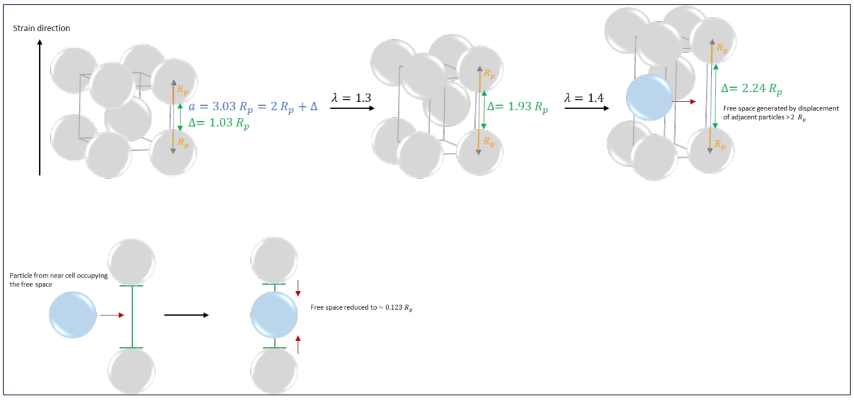

Scheme 2. Schematic representation of adjacent corner filler particle displacement along the deformation direction upon a pre-strain of 30% and the maximum of the oscillatory strain, corresponding in total to 40%. Tentative representation of particles displacement among different unit cells driven by compressive force along the direction perpendicular to the deformation.

8% double amplitude:

To verify whether the upper process is simply related to non-linearity on the level of the filler exclusively or it is valid over a wide range of dynamic amplitudes, the same experiment was conducted at lower dynamic strain amplitude corresponding to 8% peak-to-peak, i.e. 4% amplitude. In this case, a lower variation of the scattering intensity along the deformation direction is reasonably observed. Figure 4 shows that the experimental and theoretical functions for the scattering ratio are in very good agreement, indicating again an in-phase affine-like displacement of the clusters along the strain direction in the whole period of the sinusoidal deformation. In addition, the former jamming transition described for the higher deformation is not observed at this strain amplitude. Also, m>2 contributions can be excluded here and the affine-calculated behavior matches in good agreement with experiment. As consequence of the affine deformation of the aggregates, the reorganization of the fillers upon compression does not exhibit an arrest of the dynamics. This result is also corroborated by the same predictions used in the former case. The theoretical estimation $R^+ = (1 + 0.04/1.3)^D = 1.078$ assuming a value of $D = 2.5$ is in exact agreement with the ratio experimentally observed at 2s and confirms thus affine motion. Likewise, in the compressed state the calculation yields $R^- = (1 - 0.04/1.3)^D = 0.925$ which fits the experimental value for all the samples.
The comparison between the observations at 8% and 20% dynamic strain amplitudes evidences that the jamming transition is thus induced by a displacement of clusters along the strain direction with the consequent occupation of induced free space by nearby filler clusters initially located along the perpendicular direction.

Deviation from linearity could be predicted for the higher double deformation amplitude of 20%. Higher harmonics are expected for double amplitudes only exceeding 8%.
The correlation between the jamming transition and the Payne effect is identified in the relationship between the scattering data and the stress-strain loops obtained during the cycles of deformation.

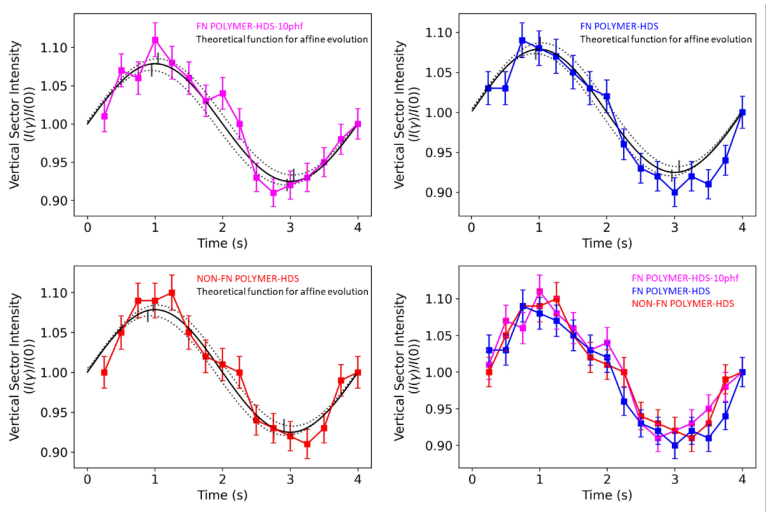

Figure 4. Evolution of the scattering ratio with 8% amplitude oscillatory deformation along the strain direction for FN POLYMER-HDS (blue), NON-FN POLYMER-HDS (red) and FN POLYMER-HDS-10phf (magenta) as function of time in comparison with the theoretical prediction of the same ratio estimated for an affine displacement of the clusters.

4.2 DMA results. LAOE stress-strain curves reported in this section were collected *in-situ* during the USAXS measurements. As this work is the first of its kind using a home-built DMA *in-situ* with scattering methods, our primary aim is the identification of specific structural features. A more quantitative study of the mechanical results will be addressed in forthcoming publications. Within this work, we limit ourselves to the semi-qualitative analysis of the hysteresis plots. The phase angles for the three samples were determined from the time-shifted normalized strain and stress signals and averaged over all cycles. While the scattering ratio function did not show a phase shift from the applied deformation, in the case of the mechanical results the phase angle was found to differ from zero. The phase angle indicated as δ is reported as function of the applied strain in Figure 5. The identification of δ values different than zero can be correlated to polymer-related contribution to the phase shift, which cannot be identified by the scattering function, purely associated to the filler displacement. A

peak in δ especially visible for sample FN POLYMER-HDS-10phf around 8% double amplitude, corroborates the Payne effect with a particular characteristic strain amplitude.

Commented [MS3]: Previous figure 5 was omitted. This new figure is related to a different aspect with respect with the previous one.

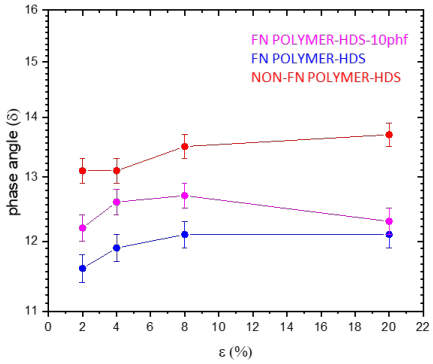

Figure 5. Phase angle as function of strain amplitude obtained for FN POLYMER-HDS (blue), NON-FN POLYMER-HDS (red) and FN POLYMER-HDS-10phf (magenta).

The full stress-strain curves at dynamic double amplitude of 8% and 20% are shown in Figure 6. The stress signals were corrected for the pre-stress as for linear rheology and the remaining dynamic stresses were plotted as function of dynamic strain. The loops for the three samples were shifted along the y axes for sake of clarity. Figure 6 (a) shows that all samples exhibit a close-to-ellipsoidal behavior for 8% amplitude, with the linear fit to the deformation loops describing the long axes. The slope of the ellipsoid gives $E^*(\omega) = \sqrt{E'(\omega)^2 + E''(\omega)^2}$ and shows no other than linear dependence of the modulus on strain. This is the signature of linear behavior. On the contrary, figure 6 (b) indicates a contribution of higher harmonics for some of the samples superposing the ground frequency for the double amplitude deformation of 20%. Whereas the area of the ellipsoidal hysteresis figures is a measure of the phase angle, its shape contains elements of non-linearities. Sample NON-FN POLYMER-HDS seems to show the largest dissipation and phase angle with the largest deviation of the linear fit from the long axes. In specific, the bending observed in the lower left corner region concerns the compression phase which in the structural part, was assigned to the jamming phenomenon for all samples.

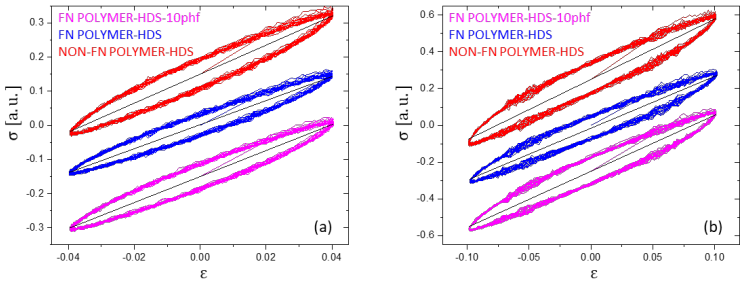

Figure 6. Stress-strain curves shifted along the vertical axes for FN POLYMER-HDS (blue), NON-FN POLYMER-HDS (red) and FN POLYMER-HDS-10phf (magenta) at sinusoidal deformation amplitude of 8% (a) and 20% (b) with related linear fit of the loops (black lines). The curves were arbitrarily shifted along the y axes for clarity.

Indeed, the absolute stresses at $\varepsilon = -0.05$ (see before for the determination) are larger than at $\varepsilon = +0.05$. The jamming causes a measurable compression force and therefore the hysteresis curves are distorted mainly in the lower left part of Figure 6. Whereas from LAOS experiments in shear the non-linearity is commonly attributed to filler phase, in the small-strain limit and polymer-related non-linear rheological behavior shows up for high amplitudes. Our work corroborates the appearance of both components in this range. The mechanical signal can be assigned to processes that are separated in origin. The observed mechanical behavior could seem, at first, in disagreement with the scattering data where a smaller displacement of clusters upon deformation was identified for sample NON-FN POLYMER-HDS with respect to the other two samples. For the interpretation of this different behavior it is important to reconsider that while the scattering measurements only relate to the effect of the deformation on the clusters, the dynamic stress-strain response is associated to the whole rubber-filler composite. The scattering function ratio evidences that in the presence of non-modified rubbers, the filler clusters are much less affected by the oscillatory deformation. A lower rubber-filler interaction in comparison to the other two samples studied, respectively FN POLYMER-HDS and FN POLYMER-HDS-10phf, leads in the case of NON-FN POLYMER-HDS to a lower dispersion of the fillers.

The lower mobility of the filler network in the case of NON-FN POLYMER-HDS is correlated to the formation of bigger clusters which occlude a significant amount of rubber. For cured composites, a lower degree of matrix functionalization is indeed known to give rise to an increase of the bound and occluded rubber amount which has a significant effect on the mechanical response. The deviation from the linear response could thus be also associated to the increased amount of bound and inside-cluster-occluded rubber. The higher mobility of the clusters being smaller and better dispersed in presence of functionalized SBR matrix might instead reduce the local stretching of polymer chains in contact with the particles within the clusters and the consequent deviation from their ideal configuration.

5. CONCLUSIONS

The combined investigation of USAXS with *in-situ* dynamic oscillatory deformation in tensile mode for differently functionalized silica-filled SBR rubbers allowed the study of filler network evolution as a function of the dynamic amplitude. The USAXS results here reported highlight a clear dependence of the cluster internal displacement and deformation under the effect of a dynamic deformation on the rubber functionalization and the dynamic amplitude of the deformation. The application of a scattering model previously defined allowed for a theoretical estimation of an affine scattering function evolution with the oscillatory deformation and its comparison with the experimental results. The filler response is purely elastic and in phase with macroscopic excitation. Non-linearities from the filler are thus localized to the filler itself and de-coupled from the rubber phase itself. The increase of rubber functionalization as well as the increase of silane amount within the composites were found to promote a close-to-affine behavior in the up-phase of the sinusoidal deformation at double amplitude of 20%, as a consequence of an enhanced filler-rubber interaction. A tentative description of the behavior makes use of the first even harmonic with m=2. A different scenario was observed for the sample containing non-functionalized SBR, where a lower-than-affine displacement of the fillers was reported. Interestingly, the down-phase of the deformation revealed a jamming transition attributed to the particle-particle contact that hinders affine rearrangement of the network in the reversed stage of the sinusoidal strain. The role of the silane was observed to be peculiar in this analysis. While the increment of the silane amount leads to closer-to-affine behavior in the up-phase, the increased matrix crosslinks might induce a hindrance of the cluster rearrangement in the reverse phase. The observation of the jamming transition at highest strain amplitude was corroborated by the analysis of the results at double dynamic amplitude corresponding to only 8%.

Author Information

Corresponding Author:
*E-mail: mariapaola.staropoli@list.lu (M.S.)
ORCID
Mariapaola Staropoli: 0000-0002-8226-8769

Dominik Gerstner (D.G.) – e-mail: dominik_gerstner@goodyear.com
Benoit Duez (B.D.) – e-mail: benoit_duez@goodyear.com
Michael Sztucki (M.Sz.) – e-mail: sztucki@esrf.fr
Guido Vehres (G.V.) – e-mail: g.vehres@fz-juelich.de
Aurel Radulescu (A.R.) – e-mail: a.radulescu@fz-juelich.de
Jean-Sébastien Thomann (J.S.T.) – e-mail: jean-sebastien.thomann@list.lu
Stephan Westermann (S.W.) – e-mail: stephan.westermann@list.lu
Wim Pyckhout-Hintzen (W.P.H.) – e-mail: w.pyckhout@fz-juelich.de

6. ACKNOWLEDGEMENT

The authors thank Goodyear S.A. for the permission to publish this paper. The present project was supported by the National Research Fund Luxembourg (IPBG16/11514551/TireMat-Tech), whose financial support is acknowledged. The authors acknowledge the ESRF of Grenoble for the provision of synchrotron radiation facilities.

References

[1] J. Domurath, M. Saphiannikova, G. Ausias, G. Heinrich, Modelling of stress and strain amplification effects in filled polymer melts, Journal of Non-Newtonian Fluid Mechanics 171-172 (2012) 8-16.

[2] A. Einstein, Eine neue Bestimmung der Moleküldimensionen, Annalen der Physik 324(2) (1906) 289-306.

[3] E. Guth, Theory of Filler Reinforcement, Journal of Applied Physics 16(1) (1945) 20-25.

[4] G. Heinrich, M. Klüppel, T.A. Vilgis, Reinforcement of elastomers, Current Opinion in Solid State and Materials Science 6(3) (2002) 195-203.

[5] S. Westermann, M. Kreitschmann, W. Pyckhout-Hintzen, D. Richter, E. Straube, B. Farago, G. Goerigk, Matrix Chain Deformation in Reinforced Networks: a SANS Approach, Macromolecules 32(18) (1999) 5793-5802.

[6] A. Botti, W. Pyckhout-Hintzen, D. Richter, V. Urban, E. Straube, A microscopic look at the reinforcement of silica-filled rubbers, The Journal of chemical physics 124(17) (2006) 174908.

[7] G. Huber, T. Vilgis, G. Heinrich, Universal properties in the dynamical deformation of filled rubbers, Journal of Physics: Condensed Matter 8 (1999) L409.

[8] A.I. Medalia, Filler Aggregates and Their Effect on Reinforcement, Rubber Chemistry and Technology 47(2) (1974) 411-433.

[9] G. Heinrich, M. Klüppel, Recent Advances in the Theory of Filler Networking in Elastomers, Filled Elastomers Drug Delivery Systems, Springer Berlin Heidelberg, Berlin, Heidelberg, 2002, pp. 1-44.

[10] R. Raghunath, D. Juhre, M. Klüppel, A physically motivated model for filled elastomers including strain rate and amplitude dependency in finite viscoelasticity, International Journal of Plasticity 78 (2016) 223-241.

[11] M. Klüppel, The Role of Disorder in Filler Reinforcement of Elastomers on Various Length Scales, in: B. Capella, M. Geuss, M. Klüppel, M. Munz, E. Schulz, H. Sturm (Eds.), Filler-Reinforced Elastomers Scanning Force Microscopy, Springer Berlin Heidelberg, Berlin, Heidelberg, 2003, pp. 1-86.

[12] B. Yin, X. Hu, K. Song, Evaluation of classic and fractional models as constitutive relations for carbon black–filled rubber, Journal of Elastomers & Plastics 50(5) (2018) 463-477.

[13] A.L. Svistkov, I.A. Morozov, STRUCTURAL-PHENOMENOLOGICAL MODEL OF THE MECHANICAL BEHAVIOR OF RUBBER, 1(1) (2010) 63-79.

[14] A. Svistkov, I. Morozov, Structural-phenomenological model of the mechanical behavior of rubber, Composites: Mechanics, Computations, Applications, An International Journal 1 (2010) 63-79.

[15] I.A. Morozov, L.A. Komar, B. Lauke, Structural–mechanical model of filled rubber: Influence of filler arrangement, International Journal of Mechanical Sciences 107(C) (2016) 160-169.

[16] Y. Isono, Nonlinear Rheology of Rubber Materials, NIPPON GOMU KYOKAISHI 86(4) (2013) 106-112.

[17] A. Lion, C. Kardelky, The Payne effect in finite viscoelasticity: constitutive modelling based on fractional derivatives and intrinsic time scales, International Journal of Plasticity 20(7) (2004) 1313-1345.

[18] A.M. Randall, C.G. Robertson, Linear-nonlinear dichotomy of the rheological response of particle-filled polymers, Journal of Applied Polymer Science 131(19) (2014).

[19] N. Warasitthinon, A.-C. GENIX, M. Sztucki, J. OBERDISSE, C.g. Robertson, The payne effect: primarily polymer-related or filler-related phenomenon?, Rubber Chemistry and Technology 92(4) (2019) 599-611.

[20] G. Kraus, Mechanical losses in carbon-black-filled rubbers, 1984.

[21] P.G. Maier, D. Goritz, Molecular interpretation of the Payne effect, Kautsch. Gummi Kunstst. 49(1) (1996) 18-21.

[22] A. Lion, Strain-Dependent Dynamic Properties of Filled Rubber: A Non-Linear Viscoelastic Approach Based on Structural Variables, Rubber Chemistry and Technology 72(2) (1999) 410-429.

[23] A.-C. GENIX, J. Oberdisse, Structure and dynamics of polymer nanocomposites studied by X-ray and neutron scattering techniques, Current Opinion in Colloid & Interface Science 20(4) (2015) 293-303.
[24] F. Ehrburger-Dolle, F. Bley, E. Geissler, F. Livet, I. Morfin, C. Rochas, Filler networks in elastomers, Macromolecular Symposia 200(1) (2003) 157-168.
[25] F. Ehrburger-Dolle, M. Hindermann-Bischoff, F. Livet, F. Bley, C. Rochas, E. Geissler, Anisotropic Ultra-Small-Angle X-ray Scattering in Carbon Black Filled Polymers, Langmuir 17(2) (2001) 329-334.
[26] K. Hagita, T. Arai, H. Kishimoto, N. Umesaki, H. Suno, Y. Shinohara, Y. Amemiya, Structural changes of silica particles in elongated rubber by two-dimensional small-angle X-ray scattering and extended reverse Monte Carlo analysis, Rheologica Acta 47 (2008) 537-541.
[27] Y.C. Lin, C.Y. Chen, H.L. Chen, T. Hashimoto, S.A. Chen, Y.C. Li, Hierarchical self-assembly of nanoparticles in polymer matrix and the nature of the interparticle interaction, The Journal of chemical physics 142(21) (2015) 214905.
[28] Y. Rharbi, B. Cabane, A. Vacher, M. Joanicot, F. Boué, Modes of deformation in a soft/hard nanocomposite: A SANS study, EPL (Europhysics Letters) 46 (2007) 472.
[29] G.J. Schneider, D. Göritz, Strain induced anisotropies in silica polydimethylsiloxane composites, The Journal of chemical physics 133(2) (2010) 024903.
[30] M. Staropoli, D. Gerstner, M. Sztucki, G. Vehres, B. Duez, S. Westermann, D. Lenoble, W. Pyckhout-Hintzen, Hierarchical Scattering Function for Silica-Filled Rubbers under Deformation: Effect of the Initial Cluster Distribution, Macromolecules 52(24) (2019) 9735-9745.
[31] B. Jiang, MODELING NONLINEAR VISCOELASTIC BEHAVIOR UNDER LARGE DEFORMATIONS, Rubber Chemistry and Technology 88(1) (2015) 28-39.
[32] C. Dessi, D. Vlassopoulos, A.J. Giacomin, C. Saengow, Elastomers in large-amplitude oscillatory uniaxial extension, Rheologica Acta 56(12) (2017) 955-970.
[33] J.B. Hipp, J.J. Richards, N. Wagner, Structure-property relationships of sheared carbon black suspensions determined by simultaneous rheological and neutron scattering measurements, Journal of Rheology 63 (2019) 423-436.
[34] D. Merger, M. Abbasi, J. Merger, A.J. Giacomin, C. Saengow, M. Wilhelm, Simple Scalar Model and Analysis for Large Amplitude Oscillatory Shear, Applied rheology 26 (2016) 53809/1-15.
[35] M. Rendek, A. Lion, Strain induced transient effects of filler reinforced elastomers with respect to the Payne-Effect: experiments and constitutive modelling, ZAMM - Journal of Applied Mathematics and Mechanics / Zeitschrift für Angewandte Mathematik und Mechanik 90(5) (2010) 436-458.
[36] M. Staropoli, D. Gerstner, A. Radulescu, M. Sztucki, B. Duez, S. Westermann, D. Lenoble, W. Pyckhout-Hintzen, Decoupling the Contributions of ZnO and Silica in the Characterization of Industrially-Mixed Filled Rubbers by Combining Small Angle Neutron and X-Ray Scattering, Polymers 12(3) (2020) 502.
[37] J. Oberdisse, Y. Rharbi, F. Boué, Simulation of aggregate structure and SANS-spectra in filled elastomers, Computational and Theoretical Polymer Science 10(1-2) (2000) 207-217.
[38] Y. Shinohara, H. Kishimoto, K. Inoue, Y. Suzuki, A. Takeuchi, K. Uesugi, N. Yagi, K. Muraoka, T. Mizoguchi, Y. Amemiya, Characterization of two-dimensional ultra-small-angle X-ray scattering apparatus for application to rubber filled with spherical silica under elongation, Journal of Applied Crystallography 40(s1) (2007) s397-s401.
[39] S. Richter, H. Kreyenschulte, M. Saphiannikova, T. Götze, G. Heinrich, Studies of the So-Called Jamming Phenomenon in Filled Rubbers Using Dynamical-Mechanical Experiments, Macromolecular Symposia 306-307(1) (2011) 141-149.
[40] C.G. Robertson, X. Wang, Isoenergetic jamming transition in particle-filled systems, Physical review letters 95(7) (2005) 075703.
[41] M. Heinrich, W. Pyckhout-Hintzen, J. Allgaier, D. Richter, E. Straube, D.J. Read, T.C.B. McLeish, D.J. Groves, R.J. Blackwell, A. Wiedenmann, Arm Relaxation in Deformed H-Polymers in Elongational Flow by SANS, Macromolecules 35(17) (2002) 6650-6664.

[42] A. Blanchard, R.S. Graham, M. Heinrich, W. Pyckhout-Hintzen, D. Richter, A.E. Likhtman, T.C.B. McLeish, D.J. Read, E. Straube, J. Kohlbrecher, Small Angle Neutron Scattering Observation of Chain Retraction after a Large Step Deformation, Physical review letters 95(16) (2005) 166001.
[43] N. Ruocco, L. Dahbi, P. Driva, N. Hadjichristidis, J. Allgaier, A. Radulescu, M. Sharp, P. Lindner, E. Straube, W. Pyckhout-Hintzen, D. Richter, Microscopic Relaxation Processes in Branched-Linear Polymer Blends by Rheo-SANS, Macromolecules 46(22) (2013) 9122-9133.
[44] T. Narayanan, M. Sztucki, P. Van Vaerenbergh, J. Leonardon, J. Gorini, L. Claustre, F. Sever, J. Morse, P. Boesecke, A multipurpose instrument for time-resolved ultra-small-angle and coherent X-ray scattering, Journal of Applied Crystallography 51(6) (2018) 1511-1524.
[45] A. Radulescu, N.K. Székely, M.S. Appavou, KWS-2: Small angle scattering diffractometer, Journal of large-scale research facilities JLSRF 1 (2015) 29.
[46] A. Thorin, A. Azoug, A. Constantinescu, Influence of prestrain on mechanical properties of highly-filled elastomers: Measurements and modeling

Influence de prédéformations sur les propriétés mécaniques d'élastomères fortement chargés: mesures et modélisation, Polymer Testing 31 (2012) 978-986.
[47] M. Wilhelm, Fourier-Transform Rheology, Macromolecular Materials and Engineering 287(2) (2002) 83-105.
[48] A.J. Giacomin, J.M. Dealy, Using large-amplitude oscillatory shear, in: A.A. Collyer, D.W. Clegg (Eds.), Rheological Measurement, Springer Netherlands, Dordrecht, 1998, pp. 327-356.
[49] J. Teixeira, Small-angle scattering by fractal systems, Journal of Applied Crystallography 21(6) (1988) 781-785.
[50] B. Hammouda, A new Guinier–Porod model, Journal of Applied Crystallography 43(4) (2010) 716-719.
[51] W. Kaewsakul, K. Sahakaro, W.K. Dierkes, J.W.M. Noordermeer, Mechanistic aspects of silane coupling agents with different functionalities on reinforcement of silica-filled natural rubber compounds, Polymer Engineering & Science 55(4) (2015) 836-842.